Physicochem. Probl. Miner. Process., 61(4), 2025, 208727

http://www.journalssystem.com/ppmp

Physicochemical Problems of Mineral Processing

ISSN 1643-1049

Enhancement of oily collector dispersion process using the confined space conditioning pulp

Yande Chao [1,2], Hainan Wang [1,3,4], Jincai Ran [5], Xiaokang Yan [1,3,4], Danlong Li [1,3,4], Haijun Zhang [1,3,4]

[1] School of Chemical Engineering and Technology, China University of Mining and Technology, Xuzhou 221116, Jiangsu, China

[2] Luanchuan Longyu Molybdenum Mining Co., Ltd., Luoyang 471500, China

[3] National Engineering Research Center of Coal Preparation & Purification, China University of Mining & Technology, Xuzhou 221116 Jiangsu, China

[4] State Key Laboratory of Coking Coal Resources Green Exploitation, China University of Mining and Technology, Xuzhou 221116, Jiangsu, China

[5] School of Mining Engineering and Geology, Xinjiang Institute of Engineering, Urumqi 830023, Xinjiang, China

Corresponding authors: zhjcumt@163.com (H. Zhang), lidlcumt@163.com (D. Li)

Abstract: Liquid–liquid mixing is generally considered as a significant prerequisite to enhance many modern industrial processes, such as mineral processing, pharmaceutical and petrochemical fields. Therein, an efficient dispersion system is required to improve the reagent adsorption and transfer behaviors, especially for the oily and insoluble collector in water. In this study, a method using the Confined-Space Pulp Conditioning Device to promote oily reagent dispersion was proposed. Different measuring points were arranged along the device wall, thus making it possible to take samples at different space and time intervals. CFD numerical simulation was employed to analyze the turbulent features of this device. Reagent concentration and droplet size distributions were obtained to evaluate the solution homogeneity. Results show that at low rotation speeds, the mixing process can reach the stable state faster but the dispersion performance is poor. With the increase of the external energy input, the mixing time required to achieve equilibrium is prolonged but both the spatiotemporal difference and the mean value of collector concentration show an obvious reduction. This finding can be associated with the dynamic evolution of oily collector dispersion under the action of turbulence. The research outcome is expected to provide important references for the optimization of liquid-liquid mixing and pulp conditioning.

Keywords: oily collector dispersion, confined space, pulp conditioning, turbulent characteristics

1. Introduction

With the minerals of high quality gradually depleted, the relatively low-grade ore has been the main target to realize the recovery of valuable components and provide raw materials for the manufacturing industry (Zheng et al., 2024). Due to the general feature of such mineral characteristics, sufficient griding is required to liberate finely disseminated constituents from unwanted gangue, thus giving rise to the increased content of small size fractions (Marion et al., 2019; Little et al., 2017; Sinnott et al., 2006). Flotation has been widely acknowledged as the main method to complete the selective separation of fine minerals, which is mainly based on the difference in surface hydrophobicity of different particles (Zhou et al., 2015; Xu et al., 2024; Wang et al., 2025). For example, hydrophobic and hydrophilic particles tend to attach to bubble surfaces and remain in pulp, respectively, which is responsible for the generation of concentrates and tailings (Chen et al., 2024; Krasowska et al., 2007; Basařová et al., 2017). During the practical flotation process, the surface hydrophobicity of objective particles is usually enhanced in the preconditioning stage through the collector adsorption (Wang et al., 2020). However, unlike the soluble reagent that can readily dissolve in pulp and interact with particle surfaces, the

DOI: 10.37190/ppmp/208727

insoluble one with poor solubility, such as the diesel, kerosene and dodecane, which has been widely applied as the collector applicable for the flotation of coal, graphite, molybdenite etc. (Chen et al., 2022; Vasumathi et al., 2023; Sun et al., 2022; Nazari et al., 2022; Gao and Pan, 2021).

In previous literature, it has been indicated that improving the pulp homogeneity can significantly contribute to the enhancement of particle surface hydrophobization (Yang et al., 2024). On the one hand, when this type of reagent is fragmentate into small droplets, larger specific surface areas can be created to achieve interaction with particles (Lian et al., 2023). On the other hand, the improved dispersion degree of oily collector can promote the collision probability between the reagents and particles but then their collision probability is expected to exhibit a decreasing trend as the collector droplet below a size threshold tends to flow around the particle without contact (Liao et al., 2020). Despite this, the decreased size of insoluble reagents is helpful for enhancing the adsorption intensity, thus giving rise to an overall positive effect on the improvement of particle surface hydrophobicity (Ma et al., 2012; Ma et al., 2013; Lai et al., 2005). As such, different methods have been employed to promote the breakup of reagents, such as increasing the energy input, emulsification and optimizing the equipment structure. Yu et al., 2017 showed that besides the pulp homogeneity, the high-intensity conditioning could also cause surface cleaning which made the fresh particle surface exposed and thus provided sites for reagent adsorption. Xia et al., 2020 introduced the collector pre-dispersion into the flotation flowsheet of low-rank coal and the flotation recovery was increased by 5-10%, which was attributed to the improved adsorption amount on the coal surface. By comparing the characteristics of stirred flow and opposite rotational flow, Li et al., 2022 demonstrated that only when the zones of high pulp homogeneity and strong strain rate were compatible with each other should the collector adsorption process be further facilitated. In addition, the oily collector was proposed to achieve strong dispersibility through emulsification, which can not only decrease the reagent consumption but also strengthen the surface hydrophobization performance (Li et al., 2024).

Despite the significant process, the distribution of insoluble reagents inside the equipment is largely unknown. Present studies mainly focus on the overall dispersion performance of collector with little attention paid to the local situation. Due to the reagent distribution readily varying with the space and time, a solid understanding for the dynamic evolution of reagent concentration inside the equipment is required. Therefore, in this study, the sampling locations are orderly placed along the Confined-Space Pulp Conditioning Device (CSPCD), which ensures the characterization of reagent concentration distribution. Additionally, CFD numerical simulation is used to explore the flow field characteristics in the confined space, including the velocity distribution, pressure distribution, turbulence kinetic energy and dissipation rate. The research outcome should have significant implications for the optimization of the equipment structure and energy input targeting liquid-liquid mixing.

2. Materials and methods

2.1. Confined-space pulp conditioning device

Pulp conditioning experiments are carried out using the Confined-Space Pulp Conditioning Device (CSPCD), and the structural diagram of this device is shown in Fig. 1. The CSPCD corresponds to a cylindrical vessel with an inner diameter of 150 mm and a height of 300 mm. The upper and lower baffles exhibit the respective inner diameter of 60 mm and 50 mm, but have the same thickness equal to 5 mm. The upper impeller is located between the top of the cylinder and the upper baffle plate, while the lower one is placed between the upper and lower baffles. The upper and lower impellers are designed as the open axial and semi-open radial types with the respective diameter equal to 55 mm and 60 mm. The distance from their centre to the device bottom is about 230 mm and 100 mm, respectively. In this study, the main operational parameter of the CSPCD corresponds to the rotation speed of impellers, which is set at 400, 800, 1200, 1600, 2000 r/min. It should be noted that two inlets are extended into the CSPCD to create colliding flow. In addition, the pressure gauge and torque sensor are introduced to measure the internal pressure of the barrel and the torque of the rotating shaft. Along the wall of the CSPCD, many rubber plugs are evenly distributed to make it possible for syringes to extract liquids during the pulp conditioning process.

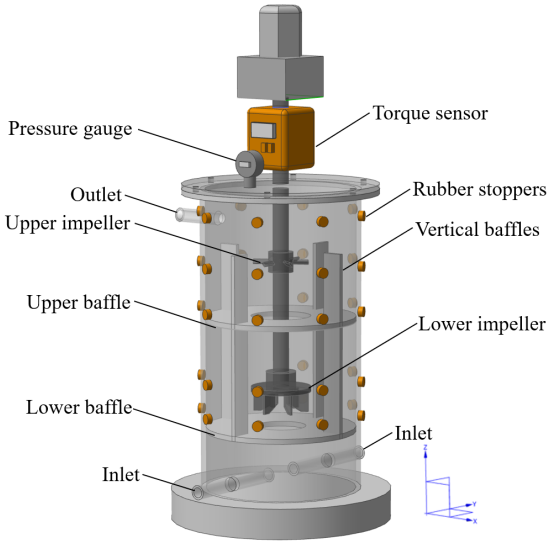

Fig. 1. Confined-Space Pulp Conditioning Device

2.2. Numerical simulation

2.2.1. Physical modelling

The geometrical model is established according to the test system shown in Fig. 1. The 3D computational basin is divided into the dynamic domain including the upper rotor and the lower rotor and the static domain including the baffle plate, and the hexahedral mesh is selected for meshing. The mesh independence is verified by taking the volume average dissipation rate as the characteristic parameter, and the mesh independence is verified as shown in Fig. 2. It can be observed that, the volume average dissipation rate increases with the increasing number of meshes, which tends to eventually stabilize after reaching 3920000. As a result, the total grid number of 3920000 is selected as the division strategy by considering both calculation accuracy and cost.

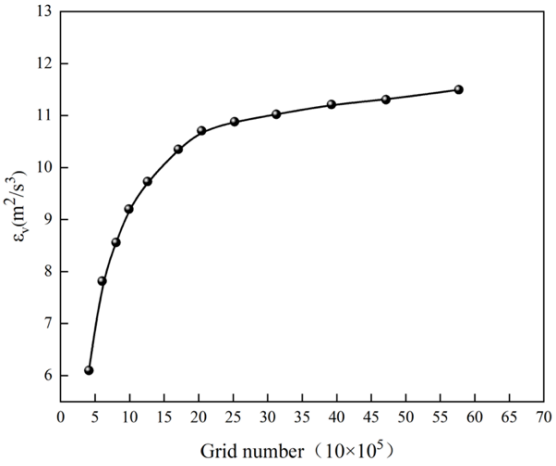

Fig. 2. Grid independence verification

2.2.2. Boundary condition

The inlet is set as mass flow inlet and the velocity of each inlet is 0.056 kg/s. The impeller rotation direction is clockwise when observed from top view and five different impeller speeds are adopted, including 400, 800, 1200, 1600, 2000 r/min. The outlet is set as the pressure outlet.

2.2.3. Computational model

Ansys Fluent software is used to numerically calculate the grid model, and the k-ε model is selected for the viscous model. The liquid aqueous phase is chosen for the fluid medium. Considering the gravity

effect, the SIMPLEC method is employed for the coupling of velocity and pressure, and the least squares cell method is used to solve the gradient. The second-order upwind scheme is adopted to solve the velocity, pressure, turbulence intensity and turbulence dissipation rate. The unsteady simulation is carried out, and the convergence accuracy is set to 10^{-4}. It is generally believed that a statistically stable state can be reached after 20 rotations of the impeller, and the flow field is set to be stable after 30 rotations of the impeller. The flow field within 10 s of the post-statistical time is taken to carry out the time-averaged analysis.

2.3. Collector dispersion experiments

During the working process of the CSPCD, the solution enters into the head-on collision zone from two feeding tubes with opposite directions, which can generate strong turbulence and promote the initial dispersion of pulp. Subsequently, the solution enters the lower impeller zone, where the strong rotation is expected to induce fluid shear for the reduction of collector droplet size. Following this, the water-oil mixture can achieve further mixing within the upper impeller zone. In addition, it should be noted that the whole process is completed under confined space. The prepared solution can be discharged from the outlet. The physical diagram of the experimental setup used for liquid-liquid mixing is shown in Fig. 3. Therein, each experiment is carried out in a stainless-steel iron system. The slurry pump was used to provide kinetic energy for feeding through the inlet, and the flowmeter was used to control the feed rate. The mixture of collector and water was returned to the tank after the mixing process through the CSPCD. During the whole experiment process, the liquid enters the CSPCD at a flow rate of 0.2 m^3/h and the impeller speed can be changed for optimization. The temperature is controlled by an air conditioner, and the investigation on collector dispersion under different conditions is completed at about 20 ℃.

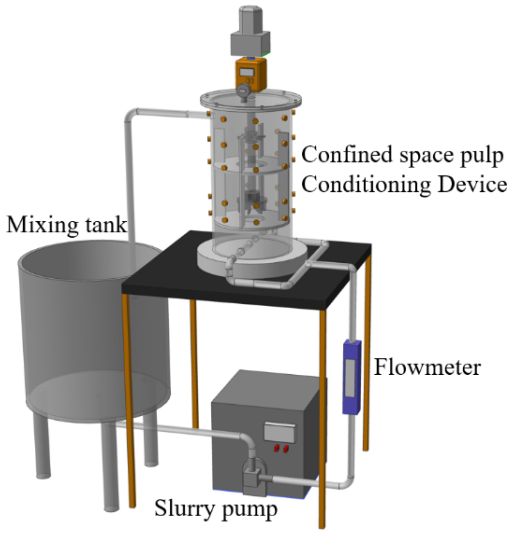

Fig. 3. The schematic layout of the pulp conditioning experimental setup

2.4. Measurement of the spatio-temporal reagent concentration

In this study, a commonly used collector in flotation, diesel oil, is selected as the research objective. Fig. 4(a) illustrates the results of Fourier Transform Infrared Spectroscopy. Therein, it can be found that the absorption peaks near 1460 cm^{-1} and 1380 cm^{-1} correspond to the C–H bending and fluoride (C–X), respectively (Uyumaz et al., 2024; Nabi et al., 2023; Yadav et al., 2015) and the absorption peak near 2798-3032 cm^{-1} is associated with the stretching vibration of -CH_n (Li et al., 2020). Such a large number of non-polar hydrocarbon groups are responsible for the poor solubility of diesel oil in water. To measure the concentration of dispersed reagents in various positions, a coloring agent is employed. Prior to the experiment, 3 g diesel oil and 0.05 g Eosin Y are mixed with 100 mL absolute alcohol to prepare the dyed collector. It should be noted that the dyed diesel oil can be diluted by deionized water to obtain different concentration, which creates the possibility to achieve the quantification of solution absorbance through the ultraviolet spectrophotometer. As such, the standard curve illustrating the

known absorbance and corresponding concentration of diesel oil can be established. The fitting result is shown in Fig. 4(b), where good consistent between the prediction and experimental data can be obtained, evidenced by the correlation coefficient larger than 0.99. During each experiment, 21 g diesel oil and 0.35 g Eosin Y are initially added into 700 mL ethanol and then mixed with deionized water to prepared 30 L solution that can be transferred to the CSPCD. The flow rate of each inlet is set at 0.2 m^3/h and the rotation speed can be controlled within the range of 400，800，1200，1600，2000 r/min. Subsequently, the syringes are used to obtain the dispersed solution at different measuring points, which can be introduced to the system of ultraviolet spectrophotometer. Notably, the concentration of diesel oil can be determined according to the standard curve in Fig. 4(b).

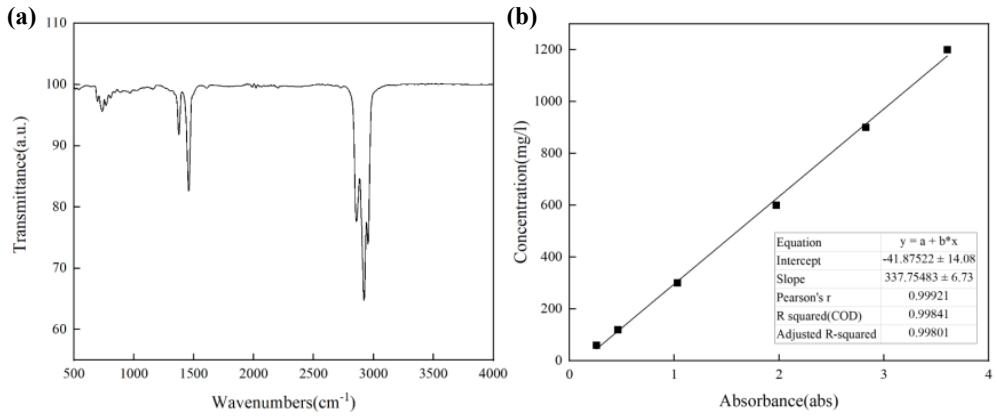

Fig. 4. (a) Infrared spectra of the diesel oil and (b) standard adsorption curves

2.5. Measurement of the spatio-temporal reagent droplet size

For each experiment, 21 g diesel oil is added into 30 L deionized water and then introduced into the CSPCD to complete the reagent dispersion. Five different impeller speeds (400，800，1200，1600，2000 r/min) can be used to carry out the conditioning process. Subsequently, the obtained solutions containing collector droplets from the CSPCD at 120 different positions are introduced to the sample delivery system of the particle size analyzer (S3500, Microtrac, US) to measure the droplet size distribution as a function of time and space.

3. Results and discussion

3.1. Flow velocity analysis

The central cross section of the CSPCD (Y=0 section) is chosen to analyze the flow velocity distribution. As shown in Fig. 5, it can be found that after entering the device, the fluids coming from two inlets are expected to collide with each other, thus giving rise to little increase in the local flow velocity within the colliding zone. Thereafter, the fluid flow is significantly affected by impeller rotation through the external energy input. It can be seen that the largest flow velocity mostly happens in the vicinity to the lower and upper impellers. As a consequence, the mixing performance of reagents should be improved. With the increase of impeller rotation speed, the fluid flow velocity in the region close to impellers exhibits an obvious increase, while that in the collision zone shows few changes. This phenomenon can be attributed to the fact that the rotor mainly influences the near-impeller area (Li et al., 2019). Although the impact of impeller rotation is enhanced under the condition of larger agitation speeds, evidenced by the enlarged region with higher fluid flow velocity, the lower part of the CSPCD is still outside the actuating range of stirred flow.

3.2. Pressure analysi

Fig. 6 presents the cloud diagram for pressure distributions varying with impeller agitation speeds at the central cross section of the CSPCD (Y=0 section). Therein, it is indicated that the pressure is larger at the lower part of the CSPCD, corresponding to the colliding zone of fluids from two inlets. The maximum pressure value is reached exactly at the center of the collision region. Accompanying the fluid

flow entering the impeller zone, the negative pressure can be produced, which is closely associated with the centrifugal force formed by the rotating motion of the lower and upper blades (Shen et al., 2021). In this scenario, the liquid tends to be thrown to the CSPCD periphery. Subsequently, the fluid is expected to collide with the baffle, thus giving rise to the velocity gradients and pressure difference. With the agitation speed increasing, the pressure in most regions of the CPSCD shows a growing trend except for the near-impeller area where the magnitude of negative pressure is further enhanced.

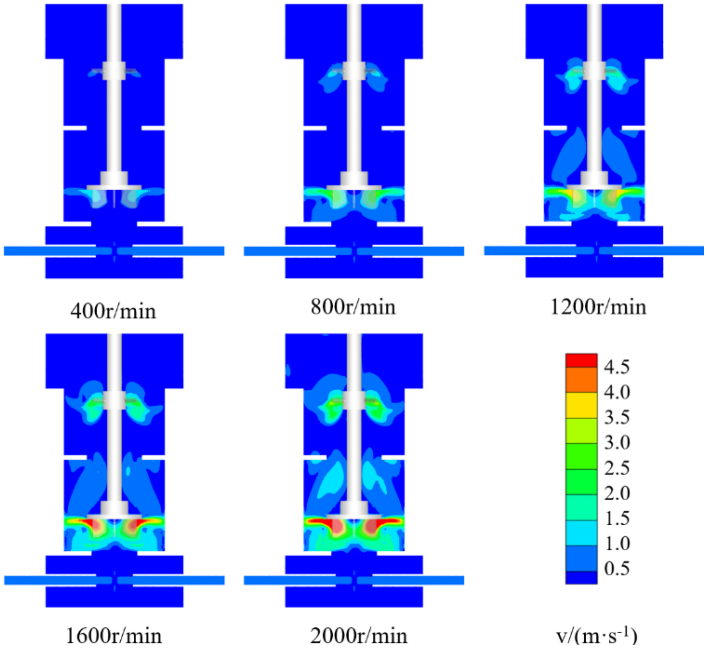

Fig. 5. Flow velocity distribution at the central cross section of the CSPCD

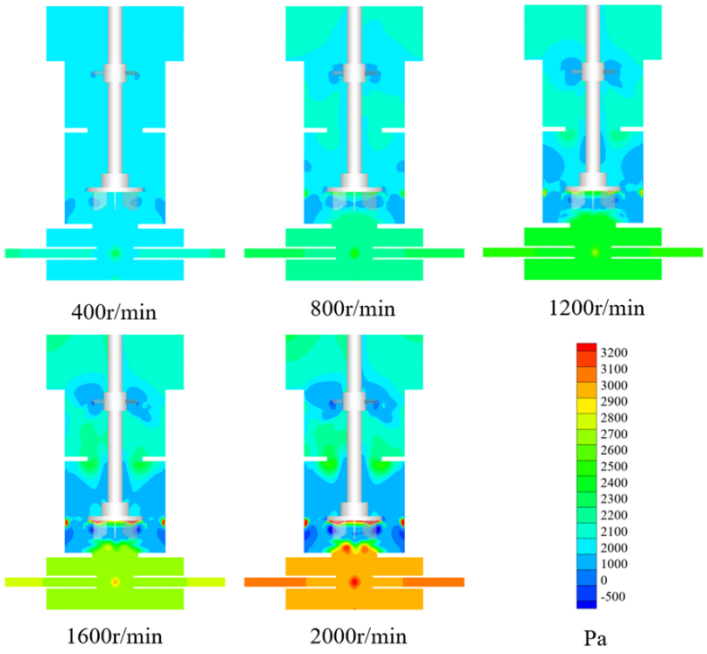

Fig. 6. Pressure distribution inside the CPSCD under different agitation speeds

In previous literature, it has been indicated that there exists a critical pressure to determine whether the two colliding droplets will coalesce with each other or bounce back (Li et al., 2023). For the case of applied pressure below this threshold, increasing pressure is helpful for increasing the droplet coalescence probability (Qian and Law, 1997). Once the produced pressure reaches the critical value, further growth of the pressure should promote the merging regime instead. Notably, it can be found

from Fig. 6 that with the increase of agitation speeds, the pressure within the head-on colliding flow region (the inlet) is increased accordingly. As a consequence, the introduction of higher agitation speeds may contribute to a larger reagent size distribution. Despite this potential effect, when the collector droplet enters the vicinity of the lower impeller, strong turbulence and fluid shear are expected to promote collector dispersion, thus giving rise to the size reduction of diesel oil.

3.3. Analysis of turbulent flow characteristics

The turbulent kinetic energy and dissipation rate changing as a function of agitation speed at the central cross section of CSPCD (Y=0 cross section) are presented in Fig. 7 (a) and 7(b), respectively. It is obvious that the distribution rules of the turbulent kinetic energy and dissipation rate are highly consistent with each other. They exhibit the maximum value within the near-impeller region. It is worth noting that the turbulent kinetic energy and turbulent dissipation rate in the CSPCD are underdeveloped when the stirring speed is 400 r/min, both of which are individually less than about 0.1 m^2/s^2 and 10 m^2/s^3. As such, it is difficult to generate high turbulence without high energy input. Notably, the increase of agitation can not only increase the turbulent intensity but also expand the actuating range of strong turbulence, characterized by the corresponding region extending from the impeller to the near-wall zone, which is favorable to the dispersion of the insoluble collector.

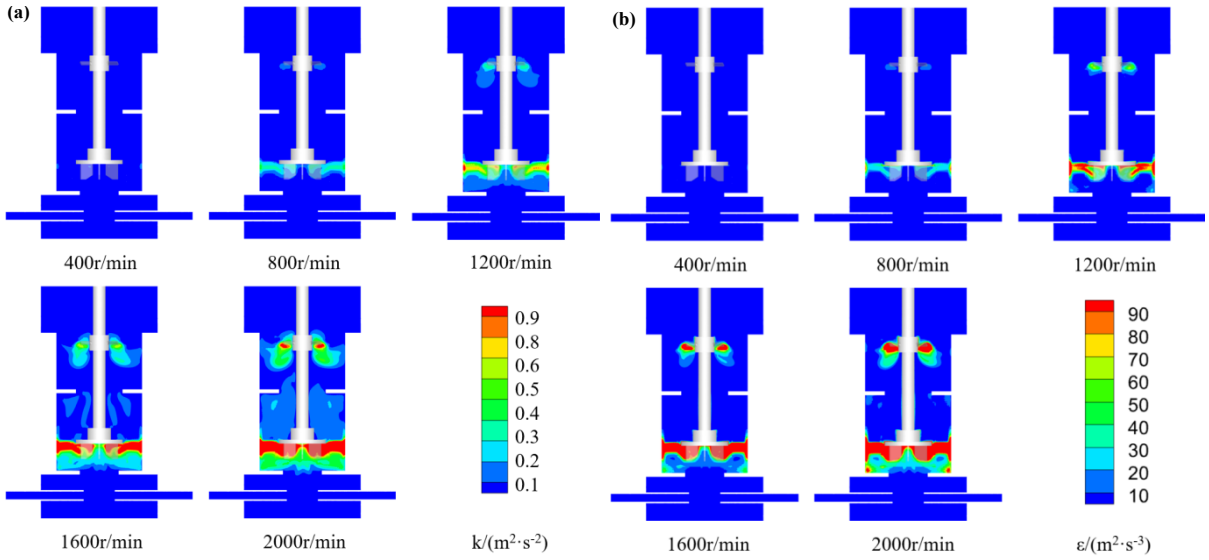

Fig. 7. Effect of agitation speed on (a) turbulent kinetic energy and (b) turbulent dissipation rate at the central cross section of the CSPCD

3.4. Analysis of the eddy scale

The common wisdom holds that turbulence can be regarded as the composition of a series of eddies in different size (Nguyen et al., 2016). Among them, the minimum eddy, known as the one with Kolmogorov length scale (η_k). As displayed in Fig. 8, the distribution of the minimum eddy at the center cross section of the CSPCD is presented under different conditions of stirring speed. It can be noted that the smallest Kolmogorov eddy is mainly distributed in the near-impeller region and the fluid collision zone, which can be associated with the strong energy dissipation. When the rotation speed is set at 400 r/min, the minimum eddy is located within the range of 30~100 μm. However, with the stirring speed increased to 2000 r/min, most areas of the CPSCD exhibit the Kolmogorov length scale less than 40 μm except for the lower part (head-on collision flow region) showing this characteristic value larger than 100 μm, which is seemingly independent on the stirring speed. This can be attributed to the fact that the inlet zone is far away from the impeller and thus minimally influenced by the external energy input.

On the one hand, in previous literature (Li et al., 2025), it has been demonstrated that particles dispersed in solution tend to be trapped by and move with the eddies have similar size to the particles. As such, the collision probability between collector droplets is expected to exhibit a corresponding increase at larger impeller speeds. On the other hand, the motion velocity of droplets can be maintained

at a certain level through the energy transfer, which can contribute to the bouncing behavior after the collision. In the meanwhile, the eddies with small scales are generally considered to exhibit high strain rate, which can give rise to the increased deformation and decreased coalescence probability because larger liquid film regions trapped between two colliding droplets are supposed to prevent the reach of critical film thickness for rupture within a limited time interval during the collisional interaction. As such, there may exist a balanced point, beyond which the collector droplet size should remain almost unchanged.

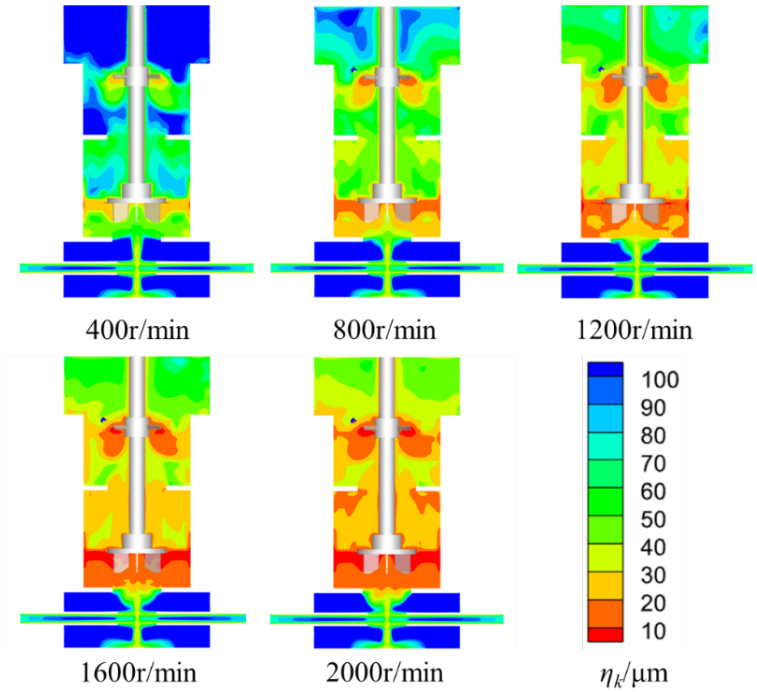

Fig. 8. Analysis of the minimum eddy scale in the CPSCD under different agitation speeds at the center cross section of the CSPCD

3.5. Spatiotemporal evolution of collector concentration

As shown in Fig. 9, the collector concentration in the CSPCD is described as a function of space under different energy input conditions. Therein, it can be observed that when the agitation speed is 400 r/min, the reagent dispersion performance is underdeveloped, evidenced by the three-dimensional collector concentration mostly larger than 600 mg/L in the device. Additionally, at relatively low agitation speeds, the difference in collector concentrations of different positions is large. Obviously, within the near-impeller regions, lower concentrations of diesel oil can be measured, while the collector in the areas far from such two impellers exhibit locally concentrated phenomenon, which can be associated with the distribution of turbulent intensity and agree well with the previous analysis of flow field characteristics. Accompanying the increase of energy input, the above effect can be alleviated. To be more specific, higher turbulent intensity in the CPSCD can induce larger fluid shear and promote the reagent dispersion. Compared with the changed reagent concentration between 540 and 600 mg/L within the near-impeller region, that in the other zones shows a larger varying range from 550 and 620 mg/L. In particular, at the rotation speed of 2000 r/min, the concentration of each measuring point is between 560 and 570 mg/L, suggesting that the uniform distribution state is basically reached. In addition, the decreased collector concentration at higher agitation speeds could also indicate the collector loss. The effect of evaporation can be excluded due to much larger boiling point of diesel oil than that of water, and the relatively short conditioning time (~2 min). Wall adhesion may be the potential reason for this effect, which can be attributed to stronger turbulent intensity at higher rotation speeds. As shown in Fig. 7, it can be found that with the rotation speed increased from 400 r/min to 2000 r/min, both the magnitude of turbulent intensity and the actuating range of impeller rotation is enhanced. Especially, when the rotation speed exceeds 800 r/min, regions with high turbulent kinetic

energy can be gradually extended to the near-wall. In this scenario, the collision probability between the collector droplet and the wall surface should be increased, which can be responsible for the collector loss.

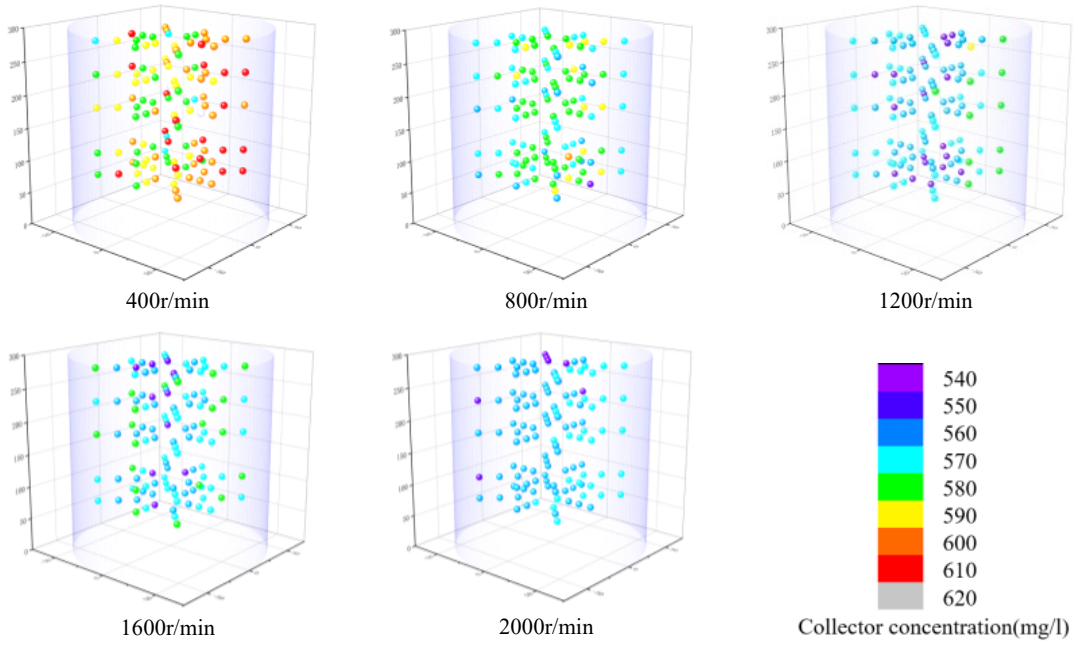

Fig. 9. Three-dimensional distribution of collector concentration varying with the stirred speed in the CSPCD

To quantitatively characterize the solution homogeneity and the difference in collector concentrations of different space, the average collector concentration in the CPSCD can be obtained based on results in Fig. 9. Following this, the uncertainty (error bar) and variance for collector concentration can be calculated, both of which can clearly show the deviation of each measuring point from the average value and indicate the degree of uniformity. As shown in Fig. 10, it can be found that the impeller speed has a significant effect on the collector concentration distribution. On the one hand, with the rotation speed increased from 400 r/min to 2000 r/min, the averaged collector concentration is decreased from 597.8 mg/L to 567.4 mg/L. On the other hand, when the impeller speed is 400 r/min, the uncertainty and variance of collector concentration are ±11.3 mg/L and 126.3 mg^2/L^2, respectively, indicating the poor dispersion effect. However, at the impeller speed of 2000 r/min, the concentration difference can be obviously narrowed, characterized by the above two factors decreasing to ± 5.2 mg/L and 27.2 mg^2/L^2, respectively. This outcome clearly suggests that increasing energy input can contribute to improving solution homogeneity and decreasing difference in collector concentrations.

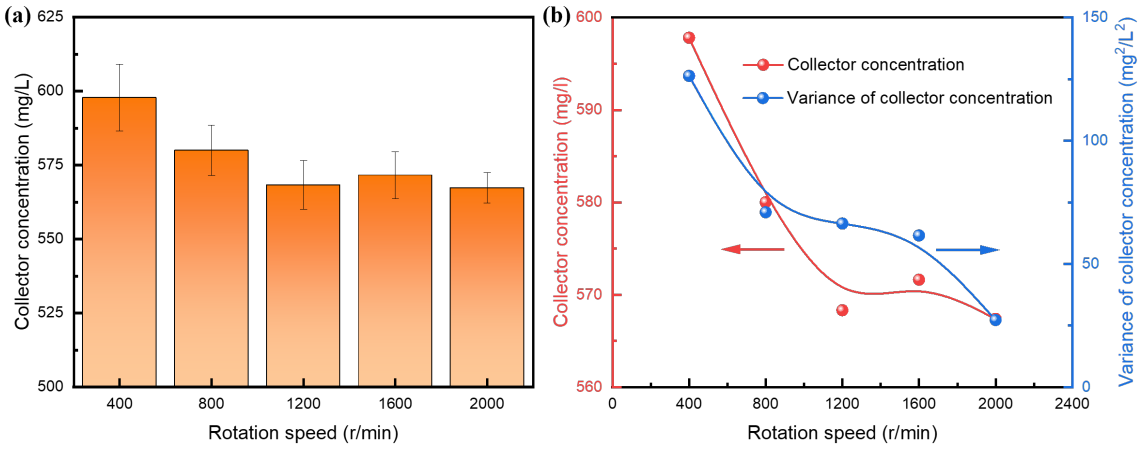

Fig. 10. Specific values of X-axis rotation speed in Fig. 10 (a) are missing. We have revised it. Please see the Email attachment

3.6. Analysis of the collector droplet size

The variation of collector droplet size at different impeller speeds and time intervals in the CSPCD is shown in Fig. 11. It is worthwhile noticing that Fig. 11(a) and 11(b) correspond to the location of the lower and upper impellers, respectively. Obviously, in two different regions, the basic variation tendency with the impeller speed is consistent with each other, characterized by the ever-decreasing collector droplet size over time. With the increased rotation speed, a larger reduction in the collector droplet size can be observed, and the final value keeps stable at a smaller level. According to the experimental measurements, in the vicinity of the lower and upper impellers, the collector droplet size requires about 60 s and 100 s to reach the equilibrium at the rotation speed of 2000 r/min, respectively, as compared to 30 s and 60 s at the rotation speed of 400 r/min. This phenomenon indicates that the collector droplet size requires more time to become smaller at higher rotation speeds, which may be attributed to more opportunities can be provided for collector to complete collision and coalescence or deformation and even breakup with the increase of external energy input. However, at the same measuring time, the collector droplet size is always decreased with increasing impeller speeds. In addition, prior to the flotation separation, pulp conditioning process is usually introduced to modulate the particle surface hydrophobicity, which can last for about 2 min or longer (Yu et al., 2017; Li et al., 2020; Wang et al., 2020). Within this time interval, the collector droplet size is expected to reach the equilibrium for the interaction with particles. It is worthwhile noticing that the error of the collector droplet size is relatively larger at the beginning but then exhibits a gradual decreasing trend, indicating the requirement for sufficient conditioning time to achieve solution homogeneity. When the equilibrium state is reached, the respective diesel oil droplet size in the vicinity of the lower impeller is about 15.5 μm and 9.8 μm at the respective rotation speed of 400 r/min and 2000 r/min. Previous literature (Chen and Peng, 2022; Zhang et al., 2024) has reported that the decreased collect droplet size is helpful for improving the flotation recovery of valuable components, hence highlighting the significance of controlling collector droplet size.

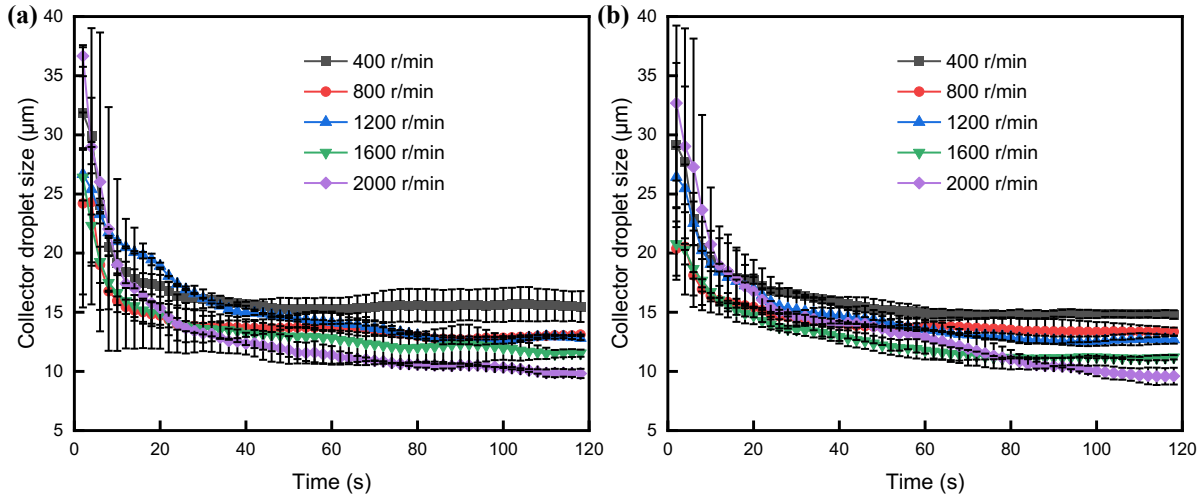

Fig. 11. Time-dependent collector droplet size at the region of the (a) lower and (b) upper impellers under different rotation speed in the CSPCD

4. Conclusions

This study is mainly devoted to providing an insight to spatiotemporal evolution of insoluble collector droplets in water by using the confined space and stirred fluid conditioning pulp. The main conclusions are presented as follows:

1. In the flow field of the CSPCD, strong turbulence can be produced within the region near the lower and upper impellers, characterized by larger fluid velocity and turbulent kinetic energy dissipation rate. In addition, due to the collision of fluids from the two inlets, local velocity gradients can be generated, thus giving rise to the improved turbulence. With the increase of rotation speed, the

influence of rotor rotation becomes gradually enhanced, including the enlarged range of strong turbulent intensity, which is conducive to dispersion of the insoluble oily collector.

2. To quantitatively obtain the three-dimensional distribution of collector concentration, different sampling points are arranged along the CSPCD. The results show that at low rotation speeds, the dispersion degree of diesel oil is underdeveloped because the corresponding flow field cannot provide sufficient fluid shear and contribute to the solution homogenization. With the increase of the impeller speed, the difference in collector distributions of different measuring points is narrowed, as well as the decreased mean value of collector concentrations, both of which demonstrate the improved mixing performance.
3. With respect to the size distribution of oily collector droplets, it is found that with the rotation speed increased from 400 to 2000 r/min, the collector droplet size exhibits a reduction from 19 to 10 μm. In addition, it should be noted that the condition of higher stirred speed requires longer time to reach the equilibrium. For example, when the rotation speed is equal to 400 r/min, it takes about 40 s to attain the stable state, as opposed to about 100 s at the speed of 2000 r/min. As such, during the practical pulp mixing process, enough time interval should be provided to complete the effective dispersion of oily collector.

Acknowledgments

This work had received the financial support from the National Natural Science Foundation of China (No. 52225405), and all authors express their sincere gratitude for it.

References

BASAROVA, P., SUCHANOVA, H., SOUSKOVA, K., VACHOVA, T., 2017, *Bubble adhesion on hydrophobic surfaces in solutions of pure and technical grade ionic surfactants*. Colloid. Surf. A, 522, 485-493.

CHEN, Y., ZHOU, B., ZHANG, X., YANG, S., HUANG, W., 2022, *Understanding the role of kerosene on the coal particle and bubble attachment process*. Fuel, 307, 121915.

CHEN, X., PENG, Y., 2022. *Physically emulsifying oily collectors to produce optimal droplet sizes for flotation*. Miner Eng. 184, 107641.

CHEN, S., WANG, J., LEI, G., MA, W., ZHANG, N., YU, Y., ZHU, Z., LI, Z., 2024. *Study on the Dynamic Process of the Attachment of a Single Bubble to Rough Surfaces with Different Hydrophobicity*. Minerals, 14, 963.

GAO, Y., PAN, L., 2021, *Understanding the mechanism of froth flotation of molybdenite using oily collectors from a perspective of thinning and rupture of thin liquid film*. Miner Eng., 163, 106805.

KRASOWSKA, M., MALYSA, K., 2007, *Kinetics of bubble collision and attachment to hydrophobic solids: I. Effect of surface roughness*. Int. J. Miner. Process., 81, 205-216.

LAI, W., XUE, Y., PANG, X., 2005, *Study on Effect of Particle Size on the Adsorption by Quantum Chemistry Method*. J. Taiyuan Univ. Technol., 36, 183-186

LI, Z., ZHAO, C., ZHANG, H., LIU, J., YANG, C., XIONG, S., 2019, *Process intensification of stirred pulp-mixing in flotation*. Chem. Eng. Process., 138, 55-64.

LI, D., ZHANG, C., LI, X., YANG, L., YAN, X., WANG, L., LIU, Q., ZHANG, H., 2020, *Experimental study on the preconditioning of fine coal particles surface modification using a new type flow mixer*. Fuel, 268, 117361.

LI, E., XIAO, X., WANG, X., PAN, Z., QIN, Y., GAO, G., DU, Z., CHENG, F., 2024, *Interfacial interaction of emulsion collector in enhancing low-rank coal flotation*. C Colloid. Surf. A, 692, 133965.

LI, D., YAN, X., WANG, W., WANG, H., ZHOU, R., YANG, H., ZHANG, H., 2022, *New insights into the intensification of collector adsorption on fine particles induced by flow field*. J. Mol. Liq., 365, 120119.

LI, M., SAHA, A., SUN, C., LAW, C.K., 2023, *Role of ambient pressure on bouncing and coalescence of colliding jets*. Phys. Fluids, 35, 31706.

LI, X., SUN, Z., WANG, H., WANG, L., YAN, X., ZHANG, H., RAN, J., LIU, J., 2025, *Particle motion under turbulent eddies: Inspiration for fine minerals flotation*. Chem. Eng. Sci., 301, 120754.

LIAN, F., LI, G., CAO, Y., ZHAO, B., ZHU, G., FAN, K., 2023, *Experimental study on the dispersion behavior of a microemulsion collector and its mechanism for enhancing low-rank coal flotation*. Int. J. Min. Sci. Technol., 33, 893-901.

LIAO, Y., HAO, X., AN, M., YANG, Z., MA, L., REN, H., 2020, *Enhancing low-rank coal flotation using mixed collector of dodecane and oleic acid: Effect of droplet dispersion and its interaction with coal particle*. Fuel 280, 118634.

LITTLE, L., MAINZA, A.N., BECKER, M., WIESE, J., 2017, *Fine grinding: How mill type affects particle shape characteristics and mineral liberation*. Min. Eng., 111, 148-157.

MA, L., WEI, L., LI, J., CHEN, Q., 2012, *Study of theory of efficient coal slurry conditioning and its application*. J. China Univ. Min. Technol., 41, 315-319

MA, L., WEI, L., ZHAO, X., CHEN, Q., 2013, *Effects of shearing strength in slurry conditioning on coal slime flotation*. J. China Coal Soc., 38, 140-144

MARION, C., LANGLOIS, R., KÖKKILIC, O., ZHOU., WILLIAMS, H., AWAIS, M., ROWSON, N.A., WATERS, K.E., 2019, *A design of experiments investigation into the processing of fine low specific gravity minerals using a laboratory Knelson Concentrator*. Min. Eng., 135, 139-155.

NABI, M.N., AKHTER, M.S., RAHMAN, M.A., 2013, *Waste Transformer Oil as an Alternative Fuel for Diesel Engine*. Proc. Eng., 56, 401-406.

NAZARI, S., ZHOU, S., HASSANZADEH, A., LI, J., HE, Y., BU, X., KOWALCZUK, P.B., 2022, *Influence of operating parameters on nanobubble-assisted flotation of graphite*. Int. J. Miner. Process., 20, 3891-3904.

NGUYEN, A.V., AN-VO, D., TRAN-CONG, T., EVANS, G.M., 2016, *A review of stochastic description of the turbulence effect on bubble-particle interactions in flotation*. Int. J. Miner. Process., 156, 75-86.

QIAN, J., LAW, C.K., 1997, *Regimes of coalescence and separation in droplet collision*. J. Fluid Mech., 331, 59-80.

SHEN, Z., 2021, *BGRIMM Mechanical Agitation Flotation Machine, Principles and Technologies of Flotation Machines*, Springer Singapore, Singapore, 213-262.

SINNOTT, M., CLRATY, P.W., MORRISON, R., 2006, *Analysis of stirred mill performance using DEM simulation: Part 1– Media motion, energy consumption and collisional environment*. Miner. Eng., 19, 1537-1550.

SUN, K., QIU, Y., ZHANG, L., LIU, Q., MAO, Z., QIAN, Y., 2022, *Enhanced fine flake graphite flotation and reduced carbon emission by a novel water-in-oil kerosene emulsion*. Colloid. Surf. A, 650, 129603.

UYUMAZ, A., AKSOY, F., SOLMAZ, H., CALAM, A., KOCAKULAK, T., ÖZGÖEN, Y.Ö., KOCER, E., AKSOY, L., 2024, *Combustion, performance and emission evaluation of a diesel engine running on microwave-assisted corn oil biodiesel mixture with carbon quantum dot nanoparticle additive*. Int. J. Hydrogen Energ., 95, 849-859.

VASUMATHI, N., SARJEKAR, A., CHANDRAYAN, H., CHENNAKESAVULU, K., REDDY, G.R., VIJAYA, T.V., EI-GENDY, N.S., GOPALKRISHNA, S.J., 2023, *A Mini Review on Flotation Techniques and Reagents Used in Graphite Beneficiation*. Int. J. Chem. Eng., 2023, 1007689.

WANG, H., YANG, W., LI, D., ZHANG, C., YAN, X., WANG, L., ZHANG, H., 2020, *Enhancement of coal flotation using impact flow conditioning pulp*. J. Clean. Prod., 267, 122124.

WANG, H., CHEN, R., LI, D., ZHANG, B., YAN, X., RAN, J., ZHANG, H., 2025, *Probing the adaptability relationship between flow characteristics and mineral particles with different size and surface hydrophobicity*. Powder Technol., 452, 120588.

XIA, Y., XING, Y., GUI, X., 2020, *Oily collector pre-dispersion for enhanced surface adsorption during fine low-rank coal flotation*. J. Ind. Eng. Chem., 82, 303-308.

XU, Q., HU, W., ZHANG, M., 2024, *High-turbulence fine particle flotation cell optimization and verification*. Sci. Rep., 14, 23124.

YADAV, S.P.R., SARAVANAN, C.G., KANNAN, M., 2015, *Influence of injection timing on DI diesel engine characteristics fueled with waste transformer oil*. Alex. Eng. J., 54, 881-888.

YANG, S., MA, W., CHAI, W., CAO, Y., 2024, H*ydrodynamics intensification and interface control in the flotation conditioning process using fractal impellers*. Sep. Purif. Technol., 328, 125043.

YU, Y., MA, L., WU, L., YE, G., SUN, X., 2017, *The role of surface cleaning in high intensity conditioning*. Powder Technol., 319, 26-33.

ZHENG, Q., DONG, L., SHEN, P., LIU, D., 2024, *Exploring a clean organic carboxylic acid depressant for flotation separation of tungsten-tin minerals*. J. Environ. Chem. Eng. 12, 113451.

ZHANG, N., RUAN, S., HAN, R., SHI, Z., ZHU, Z., YU, Y., WANG, H., LI, Z., 2024. *Enhanced flotation separation of aluminum electrolysis anode slag via microemulsification of diesel collector*. J. Mol. Liq., 399, 124414.

ZHOU, F., CHEN, T., YAN, C., LIANG, H., CHEN, T., LI, D., WANG, Q., 2015, *The flotation of low-grade manganese ore using a novel linoleate hydroxamic acid*. Colloid. Surf. A, 466, 1-9.